
Research Intership (PRe)

Field of study : Applied mathematics to physics
Scholar year : 2020-2021

# Electron diffraction : An upheaval in Crystallography

Developping an exact computation of electron scattering

Confidentiality note

Non-confidential report and publishable on the internet

*Author :*
QUACH Christine
*ENSTA Paris tutor :*
PEREZ Jerome

*Promotion:*
2022
*Host Organism Tutor:*
DREVON Tarik

Internship from 17/05/2021 to 13/08/2021

Name of the host organism: STFC
Address: Rutherford Appleton Laboratory, Harwell Campus, UK

# Acknowledgements

I want to express my deepest respect and gratitude to the CCP4's team for this opportunity and their warm welcome, especially to Pr. Eugene Krissinel, CCP4 group leader, to Dr. Martyn Winn, Computational biology group leader, and to Dr. David Waterman, Scientific Programmer.

I particularly want to express my sincere appreciation to my research supervisor Dr. Tarik Drevon, for his insightful advices and heartfelt encouragements during the study.

I also thank my dear friend Mr. Pierre Potel, without whom this internship wouldn't have been possible.

Finally, I give a heartfelt thanks to my friends and family for their warm support and love during this internship.

## Abstract

Recent trends have been to develop electron diffraction methods to study matter, especially smaller proteins' structures. This paper describes the development of an exact computational method for electron diffraction. The first step of this process focuses on the exact computation for a linear structure. The second step generalizes it for an arbitrary configuration. The results of the simulations are presented and discussed. They show the validity of the implantation. The computation can surely be improved, particularly in terms of computational complexity.

Keywords : Electron diffraction, crystallography, numerical analysis, scattering

## Résumé

Bien que la diffractométrie de rayons X ait largement faite ses preuves dans l'analyse de la structure de la matière, cette dernière ne permet pas l'étude de plus petites structures, c'est pourquoi le développement de la diffraction par électrons s'avère pertinante. Ce travail décrit le développement d'une méthode de calcul exacte de diffraction par électrons. Dans un premier temps, le processus s'attache à résoudre le problème dans le cas d'une structure linéaire, puis dans un second temps, d'une structure arbitraire. Les résultats des simulations sont présentées et analysées, et montrent la validité de la méthode d'implementation. Celle-ci pourra largement être améliorée, notament en terme de complexité de calcul.

Mots-clés : Diffraction des électrons, cristallographie, analyse numérique, diffusion des ondes

# Contents

# Liste des figures

# Introduction

In the past century, X-ray crystallography has largely been the dominating method to solve atomic and molecular structure of a crystal. But efficient though it may be, scientists have found to be limited by its poor resolving power. Recent trends have been leaning towards a new diffraction method using the electrons strong interaction with matter : electron diffraction. It has thus became crucial to better our understanding of its behaviour with matter. In this work, we develop the exact calculations of electron scattering by single organic crystal using a simplified model of the atomic electrostatic potential.

First of all, we will briefly introduce electron diffraction and the Schrodinger's equation. Secondly, we will calculate the exact solution in the linear case, and then, generalized it to the arbitrary configuration. Finally, we will look at one perspective to optimize the calculation speed.

# Chapter 1

# Electron diffraction

## 1.1 Introduction to electron diffraction

### 1.1.1 The limits of X-ray crystallography

Developed in 1920, X-ray crystallography is a largely popularized experimental method to determine the atomic and molecular structure of a crystal. Indeed, as X-rays have minimal interaction with matter, the kinematic approximation, which assimilates the diffraction figures to the 3D Fourier transform of the electronic density of the studied structure, can be used. Therefore, by doing the inverse Fourier transform, the structure of the crystal can easily be determined.

However, the main disadvantage of this method is that the X-rays have a wavelength that only allows a resolving power of the inter-atomic radius. It is therefore essential to grow the crystals to an appropriate size : to approximately the $\mu m^3$ or $cm^3$, which can be a challenge, especially in the case of proteins. This makes it very difficult to study their structure by X-ray diffraction.

### 1.1.2 Electron diffraction's challenges

Electron diffraction can thus be a very promising alternative. Indeed, very much like X-ray crystallography, electron diffraction consists in the study of the matter's structure, but instead of X-ray, it is based on the wave nature of electrons. The major perk of this method is that it allows a resolving power of approximately the nanometer, as electrons interact much more with matter. Therefore, making smaller crystals easier to study. This meth-

ods appears to be more appropriate to determine certain proteins' structure.

However, because of electrons' particular behavior with matter, the kinetic theory may not apply in this case, as the electrons are scattered several times before appearing on the screen. This is the reason why developing a computational method has become crucial to better our understanding of multiple scattering. A computation method, which simulates the multiple scattering of metals, called multislice, has already been developed, but gives approximated results. Thus, this work aims at developing an exact computational method, based on the resolution of the Schrodinger equation.

## 1.2 Scattering

### 1.2.1 Schrodinger's equation in the considered model

The Schrodinger's equation writes :

$$j\hbar\partial_t\Psi(t,\boldsymbol{r}) = \Big(-\frac{\hbar^2}{2m}\nabla^2 + V(t,\boldsymbol{r})\Big)\Psi(t,\boldsymbol{r}),$$

(i) Simplified model of the atomic electrostatic potential
In our problem, we consider a simplified model of the atomic electrostatic potential, which means that the potential energy is constant inside each quantum dot sphere.

(ii) Schrodinger's equation in the considered model
Because the potential is not time dependant, the equation then reads :

$$\Big(-\frac{\hbar^2}{2m}\nabla^2 + V(\boldsymbol{r})\Big)\Psi(\boldsymbol{r}) = E\Psi(\boldsymbol{r}).$$

It is an eigen value problem.

### 1.2.2 Solutions

In our work, we will consider the Schrodinger's equation in spherical coordinates. Thus, a family of functions solution of our eigen value problem is the family of spherical Bessel functions. These functions are comprised of 2 parts : an angular part and a radial part.

The angular function corresponds to different spherical harmonics $Y_l^m(\theta_p, \phi_p)$. They are the angular solution of the Schrodinger's equation in spherical coordinates.

The radial functions corresponds to the Bessel functions, of the first kind $j_l(kr_p)$ inside the sphere, and of the second kind, $h_l(kr_p)$, called Hankel functions, outside.

Any wave function can thus be expended on the family function $(Y_l^m(\theta_p, \phi_p)j_l(kr_p))_{lm}$ inside of the pth sphere, and $(Y_l^m(\theta_p, \phi_p)h_l(kr_p))_{lm}$ outside. (Note that a distinction is made because the Bessel function of the second kind diverges when the radius converges to 0.)

The computation of the solution, therefore, consists of finding the coefficients of expansion so that the wave function and its gradient are continue at the surface of the pth sphere.

# Chapter 2

# Linear configuration of N quantum dot spheres

In this chapter, we consider a linear configuration of N quantum dot spheres, of which we will study the diffracted field. The problem have an azimuthal symmetry. First, we will focus on the formulation of the problem, then on its implementation and verification. Finally we will apply this simulation to an example.

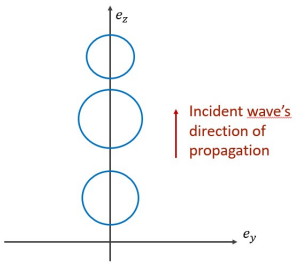


Figure 2.1: Linear configuration

## 2.1 Formulation

### 2.1.1 Scattered field

Let $a_l$ and $b_l$ be the coefficients of expansion in the family of spherical Bessel functions with an azimuthal order 0.

For $p \in [1, N]$.
The scattered wave function ***outside of the pth sphere*** is defined as :

$$f_p^{(out)}(\boldsymbol{r_p}) = \sum_{l=0}^{\infty} b_{pl} h_l(k_0 r_p) Y_l^0(\theta_p),$$

where

$$\begin{cases} k_0 = \sqrt{\frac{2m_e E_0}{\hbar^2}} & \textit{The wave number of the incident wave,} \\ E_0 & \textit{The energy of the incident wave.} \end{cases}$$

The scattered wave function ***inside of the pth sphere*** is defined as :

$$f_p^{(in)}(\boldsymbol{r_p}) = \sum_{l=0}^{\infty} a_{pl} j_l(k_p r_p) Y_l^0(\theta_p),$$

where

$$\begin{cases} k_p = k_0\sqrt{1 + \frac{V_p}{E}} & \textit{The wave number inside the pth sphere} \\ V_p & \textit{The constant potential inside the pth sphere} \end{cases}$$

The incident wave function is defined as :

$$f^{(i)}(\boldsymbol{r_p}) = e^{jk_0 d_p} c_l j_l(k_0 r_p) Y_l^0(\theta_p),$$

where

$$c_l = j^l(2l+1)\sqrt{\frac{4\pi}{2l+1}},.$$

### 2.1.2 Continuity relations

Using the continuity relation of the wave function and its gradient at the surface of the pth sphere, with $a_p$ its radius, we can deduce the expansion's coefficients $a_{pl}$ and $b_{pl}$.

$$\begin{cases} \left(\sum_{q=1}^{N} f_q^{(out)} + f^{(i)}\right)\Big|_{r_p=a_p} & = & \left(f_p^{(in)}\right)\Big|_{r_p=a_p}; \\ \partial_{r_p}\left(\sum_{q=1}^{N} f_q^{(out)} + f^{(i)}\right)\Big|_{r_p=a_p} & = & \partial_{r_p}\left(f_p^{(in)}\right)\Big|_{r_p=a_p}. \end{cases}$$

The first continuity relation gives :

$$\left(f_p^{(in)} - \sum_{q=1}^{N} f_q^{(out)}\right)\Big|_{r_p=a_p} = \left(f^{(i)}\right)\Big|_{r_p=a_p}$$

Substituting $f_p^{(in)}, f_q^{(out)}$ and $f^{(i)}$ for their developed expressions we get :

$$\sum_{l=0}^{\infty} a_{pl} j_l(k_p a_p) Y_l^0(\theta_p) - \Big( \sum_{q=1}^{N} \sum_{l=0}^{\infty} b_{ql} h_l(k_0 r_q) Y_l^0(\theta_q) \Big) \Big|_{r_p = a_p} = e^{jk_0 d_p} c_l j_l(k_0 a_p) Y_l^0(\theta_p).$$

When $q \neq p$, in the second term of the equation, we have to express the qth sphere in the $p^{th}$ frame of reference. This is why we introduce the translational addition theorem **[4][5]** :

**Translational addition theorem**

The spherical wave function $\psi_{l,m}$ from reference $O(\boldsymbol{r})$ to $O(\boldsymbol{r'})$ where $\boldsymbol{t} = \boldsymbol{r}' - \boldsymbol{r}$.

$$\psi_{l,m}^{(out)}(\boldsymbol{r}') = \sum_{\nu=0}^{\infty} \sum_{\mu=-n}^{n} a_{l,m;\nu,\mu}(\boldsymbol{t})^{(out-in)} \psi_{\nu,\mu}^{(in)}(\boldsymbol{r}),$$

with $a_{l,m;\nu,\mu}^{out-in}(\boldsymbol{t}) = 4\pi \sum_{q=|l-\nu|}^{l+\nu} (-i)^{l-\nu-q} \psi_{q,m-\mu}^{(out)}(\boldsymbol{t}) (-1)^m G(l,\nu,q,m,-\mu,-m+\mu)$, when G are the Gaunt coefficients

Thus, using the translational addition theorem for $\psi_{l,0}^{(out)} = \sum_{l=0}^{\infty} b_{ql} h_l(k_0 r_q) Y_l^0(\theta_q)$ when $q \neq p$, the equation writes :

$$\sum_{l=0}^{\infty} a_{pl} j_l(k_p a_p) Y_l^0(\theta_p) - \sum_{l=0}^{\infty} b_{pl} h_l(k_p a_p) Y_l^0(\theta_p) - \sum_{q\neq p}^{N} \sum_{n=0}^{\infty} \sum_{l'=0}^{\infty} a_{n0,l'0}^{(out)} b_{qn} j_n(k_0 a_p) Y_{l'}^{0}(\theta_p)$$
$$= e^{jk_0 d_p} c_l j_l(k_0 a_p) Y_l^0(\theta_p)$$

By multiplying the equation by $Y_l^{0*} d\Omega$ and then integrating on $\Omega$, the equation reads :

$$\int_\Omega \sum_{l=0}^{\infty} a_{pl} j_l(k_p a_p) Y_l^0(\theta_p) Y_l^{0*} d\Omega - \int_\Omega \sum_{l=0}^{\infty} b_{pl} h_l(k_p a_p) Y_l^0(\theta_p) Y_l^{0*} d\Omega$$
$$- \int_\Omega \sum_{q\neq p}^{N} \sum_{n=0}^{\infty} \sum_{l'=0}^{\infty} a_{n0,l'0}^{(out)} b_{qn} j_n(k_0 a_p) Y_{l'}^0(\theta_q) Y_l^{0*} d\Omega = \int_\Omega e^{jk_0 d_p} c_l j_l(k_0 a_p) Y_l^0(\theta_p) Y_l^{0*} d\Omega$$

Using the orthogonality of the spherical harmonics $\int_\Omega Y_l^m Y_l^{m*} d\Omega = \delta_{l,l'}^{m,m'}$ we finally get :

$$a_{pl} j_l(k_p a_p) - b_{pl} h_l(k_0 a_p) \; - j_l(k_0 a_p) \sum_{q\neq p}^{N} \sum_{n=0}^{\infty} a_{n0,l0} b_{qn} = e^{jk_0 d_p} c_l j_l(k_0 a_p)$$

Similarly the second continuity relation gives :

$$k_p a_{pl} \partial_\rho j_l(k_p a_p) - k_0 b_{pl} \partial_\rho h_l(k_0 a_p) \; - k_0 \partial_\rho j_l(k_0 a_p) \sum_{q \neq p}^{N} \sum_{n=0}^{\infty} a_{n0,l0} b_{qn} = k_0 e^{jk_0 d_p} c_l \partial_\rho j_l(k_0 a_p)$$

### 2.1.3 Far field and scattering cross section

(i) Far field

In the far field, we can make the following approximation :

$$(k_0 r_p) \approx (-j)^{l+1} \frac{e^{jk_0 rp}}{k_0 r_p}$$

Thus, the pth sphere contribution reads :

$$f_p^r(\theta) = \sum_{l=0}^{\infty} h_l(k_0 r_p) b_{pl} Y_l^0(\theta).$$

Hence,

$$f_p^r(\theta) = \sum_{l=0}^{\infty} (-j)^{l+1} \frac{e^{jk_0 rp}}{k_0 r_p} b_{pl} Y_l^0(\theta) = \frac{e^{jk_0 rp}}{k_0 r_p} f_p(\theta),$$

by defining $f_p(\theta) = (-j)^{l+1} b_{pl} Y_l^0(\theta)$.
More over, in the far field, $\theta_p \approx \theta$ and $r_p \approx r - d_p \cos\theta$. Indeed :

$$\begin{aligned} r^2 &= r_p^2 + d_p^2 + 2 r_p d_p \cos(\theta - \Theta_p) && (2.1) \\ &\approx r_p^2 \big(1 + 2 d_p / r_p \cos(\theta - \Theta_p)\big) && (2.2) \\ r &\approx r_p + d_p \cos(\theta - \Theta_p) && (2.3) \\ & && (2.4) \end{aligned}$$

Using theses approximations and the fact that the total scattering amplitude is the sum of the contribution from all individual spheres, we get :

$$f(r,\theta) = \sum_{p=1}^{N} f_p(r,\theta) = \sum_{p=1}^{N} \frac{e^{jk_0 r}}{k_0 r_p} e^{-jk_0 d_p cos(\theta)} f_p(\theta) = \frac{e^{jk_0 r}}{k_0 r_p} f(\theta),$$

where :

$$f(\theta) = \sum_{l=1}^{\infty} (-j)^{l+1} Y_l^0(\theta) \sum_{p=1}^{N} b_{pl} e^{-jk_0 d_p \cos\theta}$$

(ii) Scattering cross section

Using the definition of $f(\theta)$ and the definition of the scattering cross section :

$$\sigma = 4\pi r^2 \left| \frac{f(r,\theta)}{f^{(i)}(r,\theta)} \right|^2$$

The normalized differential scattering cross section reads :

$$\boxed{\frac{\sigma(\theta)}{\pi a_p^2} = \frac{4|f(\theta)|^2}{(k_0 a_p)^2}}$$

## 2.2 Implementation

### 2.2.1 Linear system

This system of linear equations can be rewritten in the following matrix form :

$$(\mathbb{P} - \mathbb{T})\mathbb{A} = \mathbb{L}$$

with $\mathbb{A}$ the unknown vector, $\mathbb{P}$ the matrix of each individual uncoupled sphere, $\mathbb{T}$ the cross-coupling matrix and $\mathbb{L}$ the incident wave's matrix, where :

$$\mathbb{A} = \begin{bmatrix} a_{10} \\ \vdots \\ a_{1,nmax} \\ a_{2,0} \\ \vdots \\ a_{N,nmax} \\ b_{10} \\ \vdots \\ b_{1,nmax} \\ b_{2,0} \\ \vdots \\ b_{N,nmax} \end{bmatrix}, \mathbb{P} = \begin{bmatrix} j_0(k_1a_1) & 0 & 0 & -h_0(k_0a_1) & 0 & 0 \\ & \dots & & & \dots & \\ 0 & 0 & j_M(k_Na_N) & 0 & 0 & -h_M(k_0a_N) \\ k_1\partial_\rho j_0(k_1a_1) & 0 & 0 & -\partial_\rho h_0(k_0a_1) & 0 & 0 \\ & \dots & & & \dots & \\ 0 & 0 & k_N\partial_\rho j_M(k_Na_N) & 0 & 0 & -\partial_\rho h_M(k_0a_N) \end{bmatrix},$$

$$\mathbb{L} = \begin{bmatrix} e^{jk_0d_1}c_0j_0(k_0a_1) \\ \vdots \\ e^{jk_0d_1}c_{nmax}j_{nmax}(k_0a_1) \\ e^{jk_0d_2}c_0j_0(k_0a_2) \\ \vdots \\ e^{jk_0d_N}c_{nmax}j_{nmax}(k_0a_N) \\ k_0e^{jk_0d_1}c_0\partial_\rho j_0(k_0a_1) \\ \vdots \\ k_0e^{jk_0d_1}c_{nmax}\partial_\rho j_{nmax}(k_0a_1) \\ k_0e^{jk_0d_2}c_0\partial_\rho j_0(k_0a_2) \\ \vdots \\ k_0e^{jk_0d_N}c_{nmax}\partial_\rho j_{nmax}(k_0a_N) \end{bmatrix}, \mathbb{T} = \begin{bmatrix} 0 & T_1 \\ 0 & T_2 \end{bmatrix}, \text{where } \begin{cases} T_1 = \mathbb{Q} \cdot J_1 \\ T_2 = \mathbb{Q} \cdot J_2 \end{cases},$$

$$\mathbb{Q} = \begin{bmatrix} 0 & ... & 0 & a_{00,00}(k_0d_{1N},\theta_{1N}) & ... & a_{nmax0,00}(k_0 \\ 0 & ... & 0 & a_{00,nmax0}(k_0d_{1N},\theta_{1N}) & ... & a_{n0,l0}(k_0d \\ & & & a_{n0,l0}(k_0d_{pq} & & \\ a_{00,00}(k_0d_{N1},\theta_{N1}) & ... & a_{nmax0,00}(k_0d_{N1},\theta_{N1}) & 0 & ... & 0 \\ a_{00,nmax0}(k_0d_{N1},\theta_{N1}) & ... & a_{nmax0,nmax0}(k_0d_{N1},\theta_{N1}) & 0 & ... & 0 \end{bmatrix}$$

$$J_1 = \begin{bmatrix} j_0(k_0a_1) \\ j_1(k_0a_1) \\ \vdots \\ \\ \\ \vdots \\ j_{nmax-1}(k_0a_N) \\ j_{nmax}(k_0a_N) \end{bmatrix}, J_2 = \begin{bmatrix} \partial_\rho j_0(k_0a_1) \\ \partial_\rho j_1(k_0a_1) \\ \vdots \\ \\ \\ \vdots \\ \partial_\rho j_{nmax-1}(k_0a_N) \\ \partial_\rho j_{nmax}(k_0a_N) \end{bmatrix}.$$

### 2.2.2 Analytical solution of a single quantum dot sphere scattering

Let's compute the analytical solution in the case of a single quantum dot sphere with l=0 in order to get familiar with the set of equations.

In this particular case, there is obviously no cross-coupling matrix. Hence,

the system can be written as :

$$\begin{bmatrix} j_0(k_1a_1) & -h_0(k_0a_1) \\ k_1\partial_\rho j_0(k_1a_1) & -\partial_\rho h_0(k_0a_1) \end{bmatrix} \begin{bmatrix} a_{10} \\ b_{10} \end{bmatrix} = \begin{bmatrix} e^{jk_0d_1}c_0 j_0(k_0a_1) \\ k_0e^{jk_0d_1}c_0\partial_\rho j_0(k_0a_1) \end{bmatrix}$$

Using the gaussian elimination, we finally the analytical values of $a_{10}$ and $b_{10}$ :

$$\begin{cases} a_{10} = c_0 \frac{-\partial_{k_0 r}h_0(k_0a_1)j_0(k_0a_1)+h_0(k_0a_1)\partial_{k_0 r}j_0(k_0a_1)}{k_1\partial_{k_1 r}j_0(k_1a_1)h_0(k_0a_1)-j_0(k_1a_1)\partial_{k_0 r}h_0(k_0a_1)} \\ b_{10} = c_0 \frac{-k_1\partial_{k_1 r}j_0(k_1a_1)j_0(k_0a_1)+j_l(k_pa_p)\partial_{k_0 r}j_0(k_0a_1)}{k_1\partial_{k_1 r}j_0(k_1a_1)h_0(k_0a_1)-j_0(k_1a_1)\partial_{k_0 r}h_0(k_0a_1)} \end{cases}$$

## 2.3 Validation of the implementation in the linear configuration

### 2.3.1 Continuity of the wave function

In order to validate our implementation, the continuity of the computed total wave function should be verified.

Thus, we've considered the problem with the following parameters :

$Radius\ : 3,\ 1.5,\ 3.5,\ \ Distance\ inter-spheres\ : -3, 5, 8,\ \ k_p = 1.25,\ \ nmax = 10.$

The incident, the scattered and the total wave functions have been plotted on the graphs.

From the graph we can see that the total wave function is indeed the result of the sum of the incident wave function and the computed scattered wave function. Furthermore, the total wave function seems to verify the continuity property.

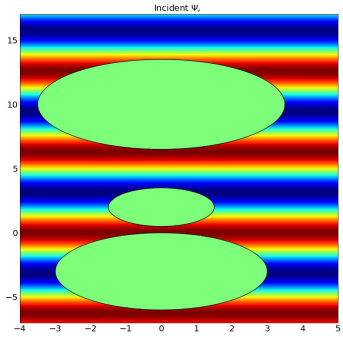


Figure 2.2: Incident wave function - Linear case

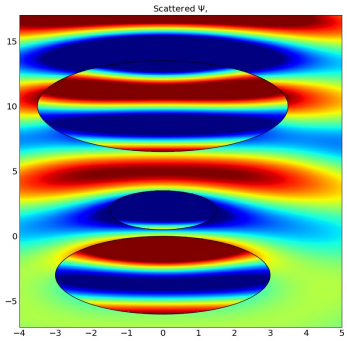


Figure 2.3: Scattered wave function - Linear case

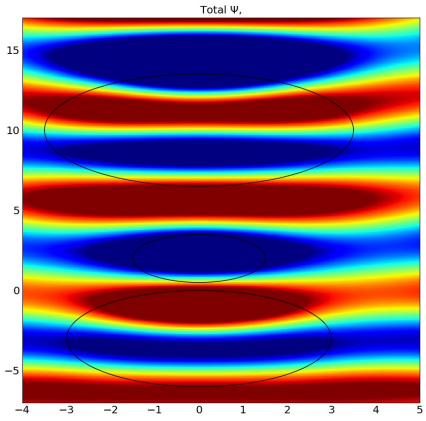


Figure 2.4: Total wave function - Linear case

In order to check more accurately the continuity, we've computed the error defined as the sum of the difference $\Psi_{|r=a_p^+} - \Psi_{|r=a_p^-}$ for each quantum dot sphere, which represents the value of the discontinuity at the edge of the spheres.

Then, the error has been plotted on the graph. The x axis indicates the maximal order Nmax and the y axis shows the logarithm of the absolute value of the error.

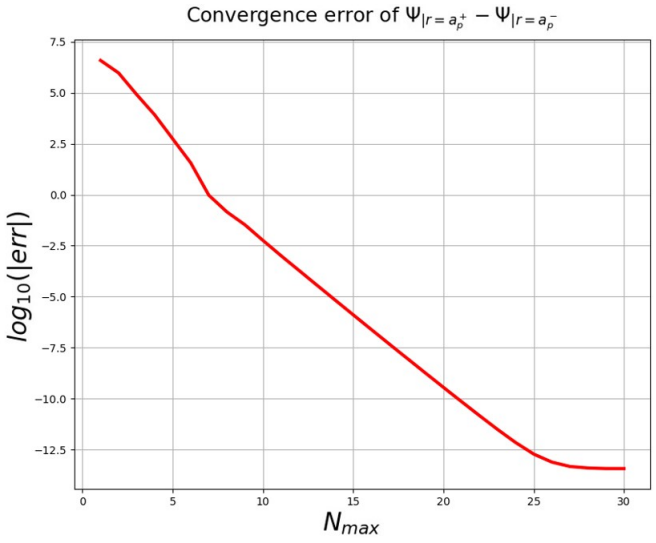


Figure 2.5: Convergence error of $\Psi_{|r=a_p^+} - \Psi_{|r=a_p^-}$ - Linear case

The graph shows that the error decreases as the value of the maximal order Nmax increase. The error's order of magnitude is approximately $10^{-10}$, which comforts us in the accuracy of our implementation.

### 2.3.2 Convergence test

Let's now check if the computed field converges to the solution. To do so, the scattering amplitude for different values for Nmax, ranging from 1 to 7 has been plotted.

As we can see, figure 2.5, from nmax=4 onward, the exact solution is computed. Thus, as expected, the computed field converges as we go up in

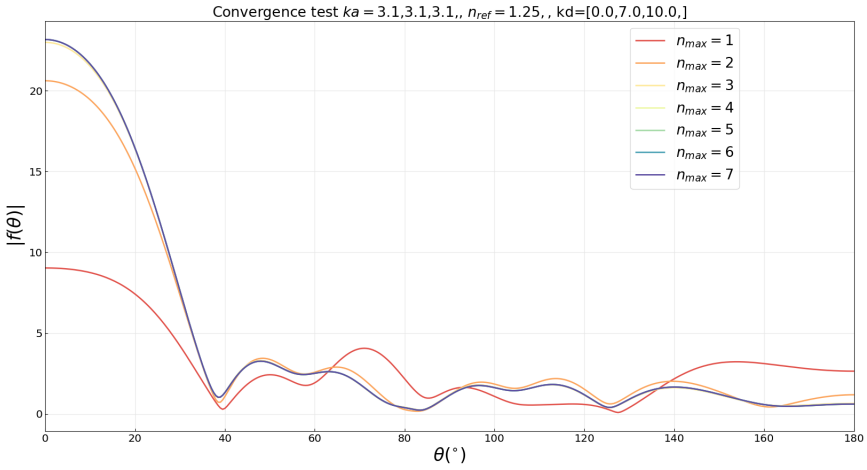


Figure 2.6: Convergence test - Linear case

orders.

## 2.4 Example case

Let's consider a case with an added perturbation of the distances between each quantum dot spheres. The considered parameters are the following :

N=5,10,20; ka(radius)=1; kd((distance inter-spheres))=2.5ka+eps, where eps varies in [0;0.5] and nref=1.1

### 2.4.1 Far field scattering

First, we've taken a look at the impact of the perturbation on the scattered field for different numbers of spheres.

The scattering amplitude has thus been plotted for each value of eps ranging from 0 to 0.5, in the case N=5,10 and 20.

From the graph we can see that the added perturbation have a relatively

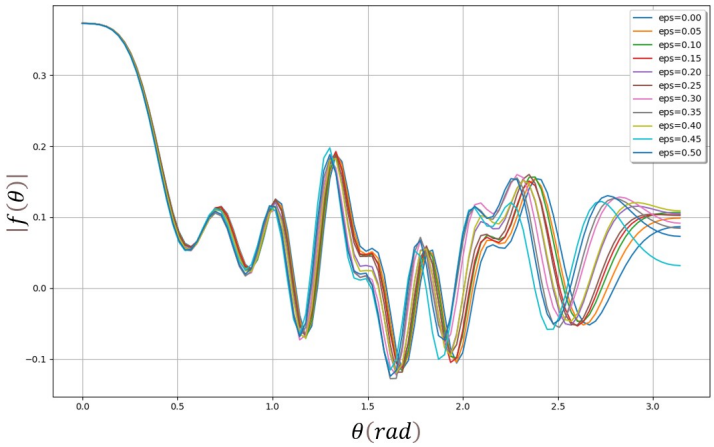


Figure 2.7: Scattering amplitude for a few eps - N=5

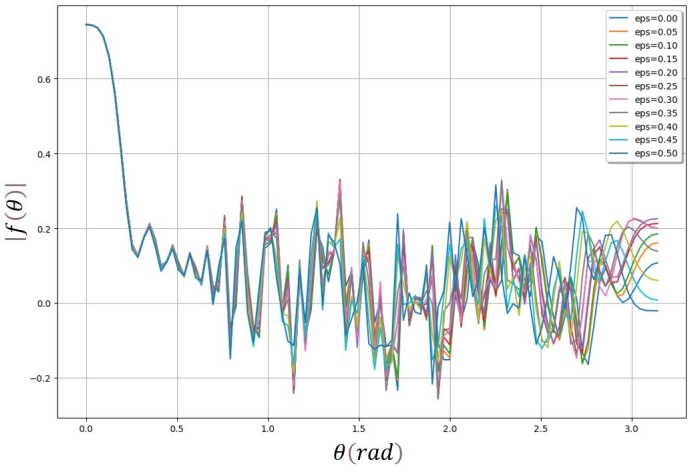


Figure 2.8: Scattering amplitude for a few eps - N=10

low impact on the scattering amplitude in the case with 5 spheres. But as the number of spheres increases, the interference seem to disappear into what looks like noise.

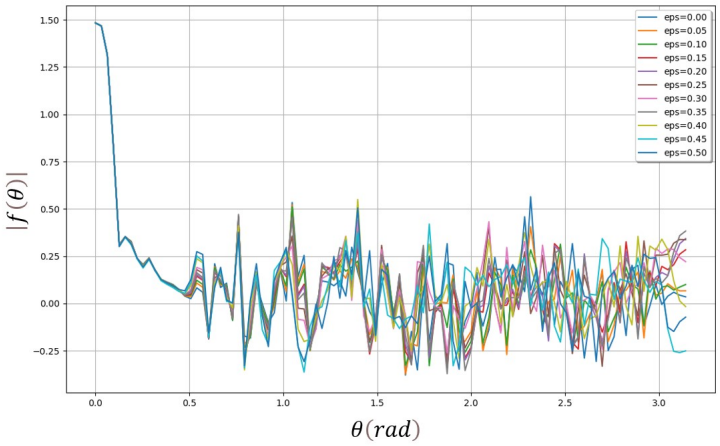


Figure 2.9: Scattering amplitude for a few eps - N=20

### 2.4.2 Scattering cross section

Secondly, we looked at how the scattering cross section behave with the added perturbation.

The scattering cross section has been plotted on the graph. The x axis indicates the values of the perturbation,eps, and the y axis shows the normalized cross section. As we can see from Figure 2.9, the scattering cross

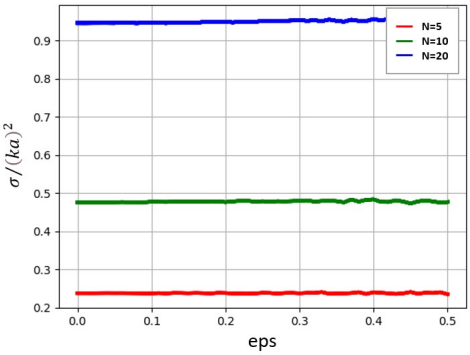


Figure 2.10: Normalized scattering cross section for randomized case - N=5,10,20

section of the total system is constant over the perturbation eps. We can

therefore deduce that the sum of each sphere's cross section is equal to the total system's cross section.

# Chapter 3

# Arbitrary configuration of N quantum dot spheres

In this third chapter, we will consider an arbitrary configuration of N quantum dot spheres. Contrary to the linear configuration, the problem has lost its azimuthal symmetry. The magnetic quantum number is now non-zero.

Similarly to the previous chapter, we will focus on the formulation of the problem, then on the implementation and finally on its validity.

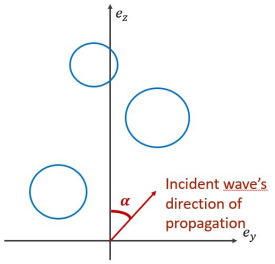


Figure 3.1: Arbitrary configuration

## 3.1 Formulation

### 3.1.1 Scattered field

By decomposing the wave function in the base of the spherical Bessel solutions, we get the following expressions :

For $p \in [1, N]$.
The scattered wave function ***outside of the pth sphere*** is defined as :

$$f_p^{(out)}(\boldsymbol{r_p}) = \sum_{l=0}^{\infty} h_l(k_0 r_p) \sum_{m=-l}^{m=l} b_{p;lm} Y_l^m(\theta_p, \phi_p),$$

where

$$\begin{cases} k_0 = \sqrt{\frac{2m_e E_0}{\hbar^2}} & \textit{The wave number of the incident wave,} \\ E_0 & \textit{The energy of the incident wave.} \end{cases}$$

The scattered wave function ***inside of the pth sphere*** is defined as :

$$f_p^{(in)}(\boldsymbol{r_p}) = \sum_{l=0}^{\infty} j_l(k_p r_p) \sum_{m=-l}^{m=l} a_{p;lm} Y_l^m(\theta_p, \phi_p),$$

where

$$\begin{cases} k_p = k_0\sqrt{1 + \frac{V_p}{E}} & \textit{The wave number inside the pth sphere} \\ V_p & \textit{The constant potential inside the pth sphere} \end{cases}$$

The incident wave function is defined as :

$$f^{(i)}(\boldsymbol{r_p}) = e^{jk_0 d_p \zeta_p} c_{lm} j_l(k_0 a_p) Y_l^m(\theta_p, \phi_p),$$

where

$$c_l = 4\pi j_l Y_l^{m*}(\alpha, \pi/2), \quad d_{pq} = |\boldsymbol{d_q} - \boldsymbol{d_p}|, \quad \zeta_p = \sin(\Theta_p)\sin(\Phi_p)\sin(\alpha) + \cos(\Theta_p)\cos(\alpha),$$

where $\alpha$ is the incidence wave's angle.

### 3.1.2 Continuity relations

Similarly to the linear configuration of N quantum dot spheres (chapter 2), using the continuity relation of the wave function and its gradient at the surface of the pth sphere, with $a_p$ its radius, we can deduce the decomposition coefficients $a_{pl}$ and $b_{pl}$.
The continuity relation reads :

$$\begin{cases} \left(\sum_{q=1}^{N} f_q^{(out)} + f^{(i)}\right)\Big|_{r_p=a_p} = \left(f_p^{(in)}\right)\Big|_{r_p=a_p}, \\ \partial_{r_p}\left(\sum_{q=1}^{N} f_q^{(out)} + f^{(i)}\right)\Big|_{r_p=a_p} = \partial_{r_p}\left(f_p^{(in)}\right)\Big|_{r_p=a_p}. \end{cases}$$

The first continuity then reads :

$$\Big(f_p^{(in)} - \sum_{q=1}^{N} f_q^{(out)}\Big)\big|_{r_p=a_p} = \Big(f^{(i)}\Big)\big|_{r_p=a_p}$$

Substituting $f_p^{(in)}, f_p^{(out)}$ and $f^{(i)}$ for their developed expressions we get :

$$\sum_{l=0}^{\infty}\sum_{m=-l}^{l} a_{p;lm} j_l(k_p a_p) Y_l^m(\theta_p,\phi_p) - \Big(\sum_{q=1}^{N}\sum_{l=0}^{\infty}\sum_{m=-l}^{l} b_{q;lm} h_l(k_0 r_q) Y_l^m(\theta_q,\phi_q)\Big)\big|_{r_p=a_p}$$

$$= e^{jk_0 d_p \zeta_p} c_{lm} j_l(k_0 a_p) Y_l^m(\theta_p,\phi_p).$$

Using the translational addition theorem**[4][5]** for $\psi_{l,m}^{(out)} = \sum_{l=0}^{\infty}\sum_{m=-l}^{l} b_{q;lm} h_l(k_0 r_q) Y_l^m(\theta_q)$ when $q \neq p$, the equation reads :

$$\sum_{l=0}^{\infty}\sum_{m=-l}^{l} a_{p;lm} j_l(k_p a_p) Y_l^m(\theta_p,\phi_p) - \sum_{l=0}^{\infty}\sum_{m=-l}^{l} b_{p;lm} h_l(k_p a_p) Y_l^m(\theta_p,\phi_p)$$

$$- \sum_{q\neq p}^{N}\sum_{\nu=0}^{\infty}\sum_{\mu=-\nu}^{\nu}\sum_{l'=0}^{\infty}\sum_{m'=-l'}^{l'} a_{\nu\mu,l'm'}^{(out)}(d_{pq},\theta_{pq},\phi_{pq}) b_{q;\nu\mu} j_\nu(k_0 a_p) Y_{l'}^{m'}(\theta_p,\phi_p) = e^{jk_0 d_p \zeta_p} c_{lm} j_l(k_0 a_p) Y_l^m(\theta_p,\phi_p)$$

By multiplying the equation by $Y_l^{m*} d\Omega$ and then integrating on $\Omega$, the equation writes :

$$\int_\Omega \sum_{l=0}^{\infty}\sum_{m=-l}^{l} a_{p;lm} j_l(k_p a_p) Y_l^m Y_l^{m*} d\Omega - \int_\Omega \sum_{l=0}^{\infty}\sum_{m=-l}^{l} b_{p;lm} h_l(k_p a_p) Y_l^m Y_l^{m*} d\Omega$$

$$- \int_\Omega \sum_{q\neq p}^{N}\sum_{\nu=0}^{\infty}\sum_{\mu=-\nu}^{\nu}\sum_{l'=0}^{\infty}\sum_{m'=-l'}^{l'} a_{\nu\mu,l'm'}^{(out)}(d_{pq},\theta_{pq},\phi_{pq}) b_{q;\nu\mu} j_\nu(k_0 a_p) Y_{l'}^{m'} Y_l^{m*} d\Omega$$

$$= \int_\Omega e^{jk_0 d_p \zeta_p} c_{lm} j_l(k_0 a_p) Y_l^m Y_l^{m*} d\Omega$$

Using the orthogonality of the spherical harmonics $\int_\Omega Y_l^m Y_{l'}^{m'*} d\Omega = \delta_{l,l'}^{m,m'}$ we finally get :

$$a_{p;lm} j_l(k_p a_p) - b_{p;lm} h_l(k_0 a_p) - j_l(k_0 a_p) \sum_{q\neq p}^{N}\sum_{\nu=0}^{\infty}\sum_{\mu=-\nu}^{\mu=\nu} a_{\nu,\mu;l,m}^{(out-in)} b_{q;\nu\mu} = e^{jk_0 d_p \zeta_p} c_{lm} j_l(k_0 a_p).$$

The second continuity relation gives :

$$k_p a_{p;lm}\partial_\rho j_l(k_p a_p) - k_0 b_{p;lm}\partial_\rho h_l(k_0 a_p) - k_0 \partial_\rho j_l(k_0 a_p) \sum_{q\neq p}^{N}\sum_{\nu=0}^{\infty}\sum_{\mu=-\nu}^{\mu=\nu} a_{\nu,\mu;l,m}^{(out-in)} b_{q;\nu\mu}$$

$$= k_0 e^{jk_0 d_p \zeta_p} c_{lm}\partial_\rho j_l(k_0 a_p)$$

## 3.2 Implementation of an arbitrary N quantum dot spheres

### 3.2.1 Linear system

This system of linear equations can be rewritten in the following matrix form :

$$(\mathbb{P} - \mathbb{T})\mathbb{A} = \mathbb{L},$$

with $\mathbb{A}$ the unknown vector, $\mathbb{P}$ the matrix of each individual uncoupled sphere, $\mathbb{T}$ the cross-coupling matrix and $\mathbb{L}$ the incident wave's matrix, where :

$$\mathbb{A} = \begin{bmatrix} a_{100} \\ \dots \\ a_{10m} \\ \dots \\ a_{1,nmax,nmax} \\ a_{2,0,0} \\ \dots \\ a_{2,0,m} \\ \dots \\ a_{N,nmax,nmax} \\ b_{1,0-nmax} \\ \dots \\ b_{10m} \\ \dots \\ b_{1,nmax,nmax} \\ b_{2,0,0} \\ \dots \\ b_{2,0,m} \\ \dots \\ b_{N,nmax,nmax} \end{bmatrix}, \mathbb{L} = \begin{bmatrix} e^{jk_0 d_1 \zeta_1} c_{00} j_0(k_0 a_1) \\ \dots \\ e^{jk_0 d_1 \zeta_1} c_{0m} j_0(k_0 a_1) \\ \dots \\ e^{jk_0 d_1 \zeta_1} c_{nmax,nmax} j_{nmax}(k_0 a_1) \\ e^{jk_0 d_2 \zeta_2} c_{00} j_0(k_0 a_2) \\ \dots \\ e^{jk_0 d_2 \zeta_2} c_{0m} j_0(k_0 a_2) \\ \dots \\ e^{jk_0 d_N \zeta_p} c_{nmax,nmax} j_{nmax}(k_0 a_N) \\ k_0 e^{jk_0 d_1 \zeta_1} c_{00}\partial_\rho j_0(k_0 a_1) \\ \dots \\ k_0 e^{jk_0 d_1 \zeta_1} c_{0m}\partial_\rho j_0(k_0 a_1) \\ \dots \\ k_0 e^{jk_0 d_1 \zeta_1} c_{nmax,nmax}\partial_\rho j_{nmax}(k_0 a_1) \\ k_0 e^{jk_0 d_2 \zeta_2} c_{00}\partial_\rho j_0(k_0 a_2) \\ \dots \\ k_0 e^{jk_0 d_2 \zeta_2} c_{0m}\partial_\rho j_0(k_0 a_2) \\ \dots \\ k_0 e^{jk_0 d_N \zeta_p} c_{nmax,nmax}\partial_\rho j_{nmax}(k_0 a_N) \end{bmatrix},$$

$$\mathbb{T} = \begin{bmatrix} 0 & T_1 \\ 0 & T_2 \end{bmatrix}, \text{ where } \begin{cases} T_1 = \mathbb{Q} \cdot J_1 \\ T_2 = \mathbb{Q} \cdot J_2 \end{cases},$$

$$\mathbb{Q} = \begin{bmatrix} 0 & ... & 0 & a_{\nu\mu,lm}(k_0 d_{pq}, \theta_{pq}) & ... & a_{\nu\mu,lm}(k_0 d_{pq}, \theta_{pq}) \\ 0 & ... & 0 & a_{\nu\mu,lm}(k_0 d_{pq}, \theta_{pq}) & ... & a_{\nu\mu,lm}(k_0 d_{pq}, \theta_{pq}) \\ & & & & & \\ a_{\nu\mu,lm}(k_0 d_{pq}, \theta_{pq}) & ... & a_{\nu\mu,lm}(k_0 d_{pq}, \theta_{pq}) & 0 & ... & 0 \\ a_{\nu\mu,lm}(k_0 d_{pq}, \theta_{pq}) & ... & a_{\nu\mu,lm}(k_0 d_{pq}, \theta_{pq}) & 0 & ... & 0 \end{bmatrix}$$

$$J_1 = \begin{bmatrix} j_0(k_0 a_1) \\ j_0(k_0 a_1) \\ ... \\ j_{nmax}(k_0 a_1) \\ j_{nmax}(k_0 a_1) \\ ... \\ j_{nmax}(k_0 a_N) \\ j_{nmax}(k_0 a_N) \end{bmatrix}, \; J_2 = \begin{bmatrix} \partial_\rho j_0(k_0 a_1) \\ \partial_\rho j_0(k_0 a_1) \\ ... \\ \partial_\rho j_{nmax}(k_0 a_1) \\ \partial_\rho j_{nmax}(k_0 a_1) \\ ... \\ \partial_\rho j_{nmax}(k_0 a_N) \\ \partial_\rho j_{nmax}(k_0 a_N) \end{bmatrix},$$

$$\mathbb{P} = \begin{bmatrix} j_0(k_1 a_1) & 0 & 0 & -h_0(k_0 a_1) & 0 & 0 \\ & ... & & & ... & \\ 0 & 0 & j_M(k_N a_N) & 0 & 0 & -h_M(k_0 a_N) \\ n_1 \partial_\rho j_0(k_1 a_1) & 0 & 0 & -\partial_\rho h_0(k_0 a_1) & 0 & 0 \\ & ... & & & ... & \\ 0 & 0 & n_N \partial_\rho j_M(k_N a_N) & 0 & 0 & -\partial_\rho h_M(k_0 a_N) \end{bmatrix}.$$

## 3.3 Validation of the implementation

### 3.3.1 Continuity of the wave function

Similarly as the linear case, in order to validate our implementation, the continuity of the computed total wave function should be verified.
Thus, we've considered the problem with the following parameters :

$$Radius \; : [2.4, 4, 2.4], \quad Distance \; inter-spheres \; : z : [5, -4.5, 4.5], \; y : [0, 4.5, 4.5]$$

$$k_p = 1.25, \quad nmax = 7.$$

The incident, the scattered and the total wave functions have been plotted on the graphs.

As we can see from the Figure 3.4, the total wave function seems to verify the continuity condition, which comforts us in our implementation.

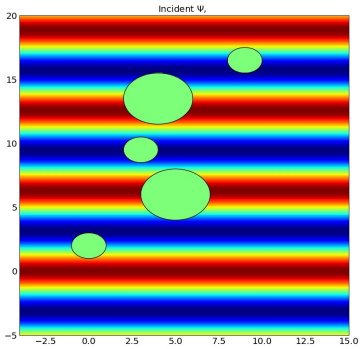


Figure 3.2: Incident wave function - Arbitrary case

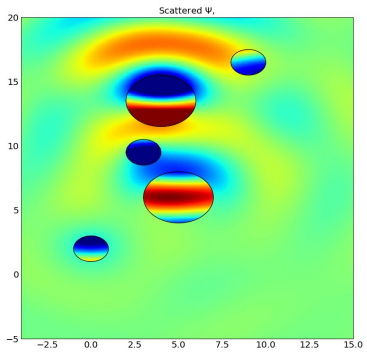


Figure 3.3: Scattered wave function - Arbitrary case

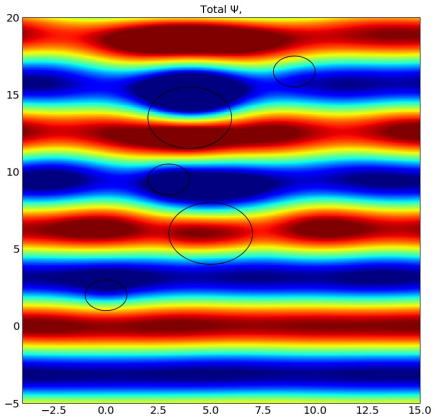


Figure 3.4: Total wave function - Arbitrary case

In order to have a more accurate look at the continuity of the computed field at the edge of each spheres, we've defined the error as sum of the difference $\Psi_{|r=a_p^+} - \Psi_{|r=a_p^-}$ on each quantum dot sphere.

The error has thus been plotted on the graph. The x axis indicates the maximal order Nmax and the y axis shows the logarithm of the absolute value of the error.

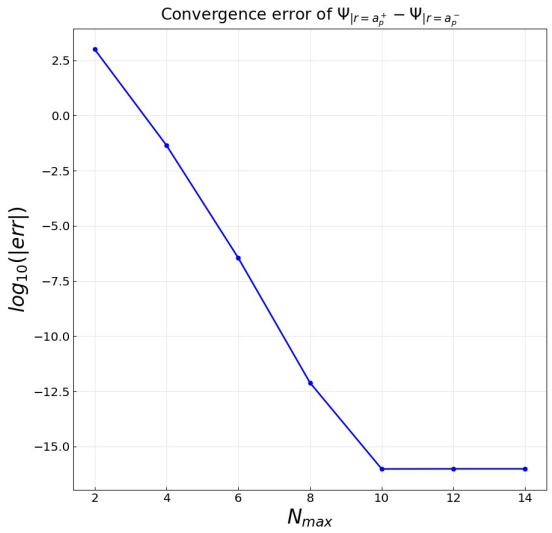


Figure 3.5: Convergence error of $\Psi_{|r=a_p^+} - \Psi_{|r=a_p^-}$ - Arbitrary case

From the graph we can see that the error decreases as the order goes up. It even reaches a plateau at $10^{-16}$ which corresponds to the order of magnitude of a machine precision. We can thus be confident in the validity of our implementation.

### 3.3.2 Convergence test

The continuity of the computed field has been checked, now let's see if the implementation allows the computed field to convergence towards the solution.
The scattered far field for different values of $n_{max}$ ranging from 1 to 8 has been plotted on the graph. The x axis indicates the angle $\theta$ and the y axis shows the amplitude of the field.

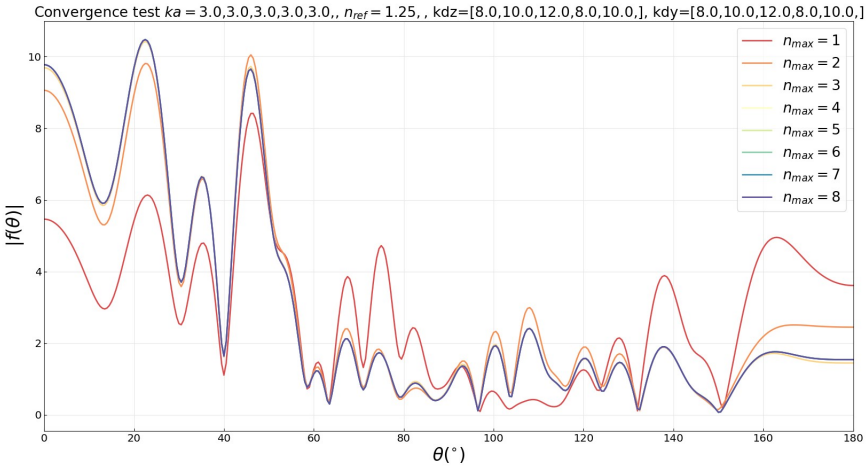


Figure 3.6: Convergence test - Arbitrary case

The graph shows that from Nmax=4 onward, the exact solution is computed. We can therefore conclude with confidence that the computed field converges towards the solution.

# Chapter 4

# Optimization of the computational speed

In this last chapter we will focus on the optimization of the field computation's speed. We will first look at a more adapted implementation of spherical harmonics, then run speed tests.

## 4.1 Implementation of the spherical harmonics

In the original code, the spherical harmonics were computed using the library scipy.special whose function, *sph_harm*, computed the spherical harmonics, for l and m, and the position $\theta$ and $\phi$ given, defined as :

$$Y_l^m(\theta,\phi) = \sqrt{\frac{2n+1}{4\pi}\frac{(n-m)!}{(n+m)!}}e^{im\phi}P_l^m(cos(\theta)).$$

$P_l^m$ are the associated Legendre polynomials, computed by solving the following differential equation :

$$P_l^m(x) = (-1)^m(1-x^2)^{m/2}\frac{\mathrm{d}^m}{\mathrm{d}x^m}P_l(x),$$

where

$$P_l(x) = \sum_{k=0}^{\infty}\frac{(-l)_k(l+1)_k}{(k!)^2}(\frac{1-x}{2})^k.$$

This process majorly affected the computational speed as it requires to solve the differential equation for each and every value of l ranging from 0 to nmax and m between -l and l to compute the spherical harmonics.

Thus, using a recurrence formula to compute the spherical harmonics on the fly seemed like a more suitable option for our problem.

### 4.1.1 Legendre polynomials recurrence formula

(i) Theory

The Legendre polynomials $P_l^m$ can be computed using the following recurrence formula :

Initialization :

$$\begin{cases} P_0^0(x) = 1 \\ P_1^1(x) = -(1-x^2)^{1/2} \\ P_0^{-1}(x) = -\frac{1}{2}P_1^1(x) \end{cases}$$

For $l > 0$ :

$$\begin{cases} P_{l+1}^{l+1}(x) = -(2l+1)\sqrt{1-x^2}P_l^l(x) \quad for\ m = l \\ (l-m+1)P_{l+1}^m(x) = (2l+1)xP_l^m(x) - (l+m)P_{l-1}^m(x) \quad for\ m \neq l \end{cases}$$

(ii) Implementation

As the computation of the field requires each value of the spherical harmonics for l and m, the Legendre polynomials are implemented in a matrix assembled as :

$$\begin{bmatrix} P_0^0 & 0 & 0 & 0 & 0 & 0 & 0 & 0 & 0 \\ P_1^0 & P_1^1 & 0 & 0 & 0 & 0 & 0 & 0 & P_1^{-1} \\ P_2^0 & P_2^1 & P_2^2 & 0 & 0 & 0 & 0 & P_2^{-2} & P_2^{-1} \\ P_3^0 & P_3^1 & P_3^2 & P_3^3 & 0 & 0 & P_3^{-3} & P_3^{-2} & P_3^{-1} \\ P_4^0 & P_4^1 & P_4^2 & P_4^3 & P_4^4 & P_4^{-4} & P_4^{-3} & P_4^{-2} & P_4^{-1} \end{bmatrix},$$

using the recurrence formula. The following spherical harmonics are thus computed using the previous ones.

This implementation method then allows to output the computation of the spherical harmonics out of the 2 for loops on l and m.

### 4.1.2 Validation

In order to validate our implementation, we compare the spherical harmonics computed by the *scipy.special.sph_harm* function to our implementation using the recurrence formula.

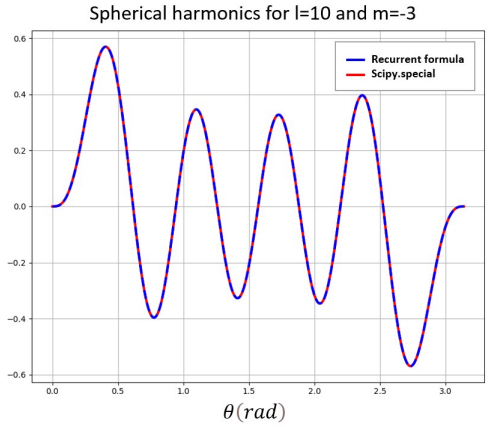


Figure 4.1: Spherical harmonics for l=10, m=-3

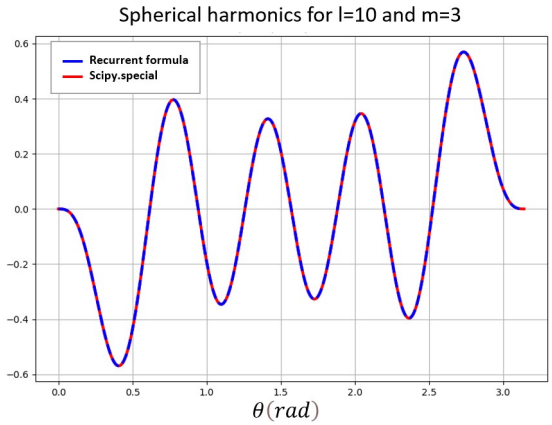


Figure 4.2: Spherical harmonics for l=10, m=3

In the example bellow, the spherical harmonics are computed for l=10 and m=-3 and 3, where $\phi = 0$ and $\theta \in [0; \pi]$

## 4.2 Speed tests

### 4.2.1 Speed tests on spherical harmonics and scattered field

(i) Computation of the spherical harmonics

We compare the computational speed of the two different methods, in the case where the spherical harmonics are calculated for $\phi = 0$, $\theta \in [0, \phi]$ and l=10 (which corresponds to the maximum value generally needed to compute the scattered field) and $\in [-l, l]$.

| | Recurrence formula | Scipy's function |
|---|---|---|
| Spherical harmonics | 0.004826784133911133 s | 0.16061711311340332 s |

As shown in the table, using the recurrence formula implementation allows a gain of 3 orders of magnitude in speed, which is not negligible.

(ii) Computation of the scattered field

Let's see if there is an actual gain in speed in the scattered field computation.

| | Recurrence formula | Scipy's function |
|---|---|---|
| Scattered field | 20.19532084465027 s | 25.091874837875366 s |

This time, the recurrence formula implementation doesn't give a significant gain in speed.

## 4.3 Discussion and perspectives of improvement

As we can see from table 2, there is not a significant gain of time in the computation of the speed, or at least not as much as expected, meaning that the computation speed is slowed down by an other element in the code.

Another possibility could come from the fact that because when we use the translational addition theorem in the code, the Gaunt coefficients have to be computed one by one for each value of l and m using the sage.math library, which slows down the computational speed. A perspective of improvement could be to implement the computation of these coefficients, using a vectoralized function.

Moreover, an alternative solution could also be to implement the computation that in C++ language, using fortran, to gain computational speed.

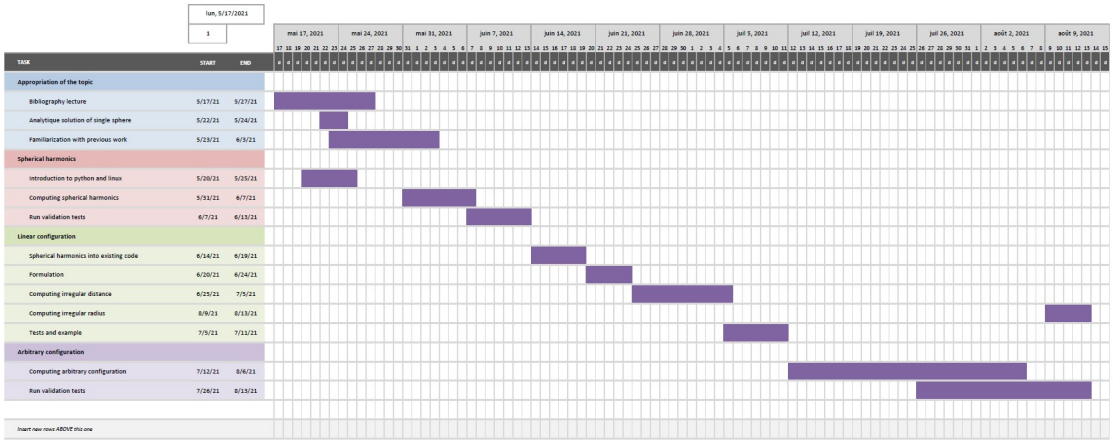


Figure 4.3: Gantt chart

# Conclusion

In this work, a brief introduction of electron diffraction and its challenges was made, stressing the importance of developing new exact methods to solve Schrodinger's equation. The exact computation of a linear configuration of N quantum dot spheres has been presented, and generalized to the arbitrary case. The implementation has then been verified, and its speed performances have been tested. It was made clear that results could surely be improved, especially in terms of computational complexity.

On a more personal level, this internship has allowed me to catch an accurate glimpse of what the world of research looks like. Moreover, this work has been fundamentally important as it has helped me grow a deeper interest in the field of physics and computational science.

# Bibliography

[**1**] Hamid, A.-K., Ciric, I. R., Hamid, M. (1990). Electromagnetic scattering by an arbitrary configuration of dielectric spheres. Canadian Journal of Physics, 68(12), 1419–1428. https://doi.org/10.1139/p90-203

[**2**] Silva, G. T., Baggio, A. L., Lopes, J. H., Mitri, F. G. (2014). Exact computations of the acoustic radiation force on a sphere using the translational addition theorem. ArXiv:1210.2116 [Physics]. http://arxiv.org/abs/1210.2116

[**3**] Hamid, A.-K., Ciric, I. R., Hamid, M. (1990). Multiple scattering by a linear array of conducting spheres. Canadian Journal of Physics, 68(10), 1157–1165. https://doi.org/10.1139/p90-163

[**4**] Batool, S., Frezza, F., Mangini, F., Yu-Lin, X. (2020). Scattering from multiple PEC sphere using Translation Addition Theorems for Spherical Vector Wave Function. Journal of Quantitative Spectroscopy and Radiative Transfer, 248, 106905. https://doi.org/10.1016/j.jqsrt.2020.106905

[**5**] Dufva, T. J., Sarvas, J., Sten, J. C.-E. (2008). UNIFIED DERIVATION OF THE TRANSLATIONAL ADDITION THEOREMS FOR THE SPHERICAL SCALAR AND VECTOR WAVE FUNCTIONS. Progress In Electromagnetics Research B, 4, 79–99. https://doi.org/10.2528/PIERB07121203

[**6**]GitHub, pyScatSpheres' code, URL : https://github.com/ronandrevon/pyScatSpheres

[**7**]ReadToDocs, pyScatSpheres' documentation,
URL : https://github.com/ronandrevon/pyScatSpheres

# Glossary

**Diffraction** : Phenomena that occur when a wave encounters an obstacle or opening

**Scattering** : Physical processes where moving particles are forced to deviate from a straight trajectory by localized non-uniformities in the medium through which they pass.

**Quantum dot** : Semiconductor particles a few nanometres in size, having optical and electronic properties that differ from larger particles due to quantum mechanics.